Advances in bromate reduction by heterogeneous photocatalysis: The use of a static mixer as photocatalyst support

Daniela F.S. Morais, Rui A.R. Boaventura, Francisca C. Moreira*, Vítor J.P. Vilar*

Laboratory of Separation and Reaction Engineering – Laboratory of Catalysis and Materials (LSRE-LCM), Departamento de Engenharia Química, Faculdade de Engenharia, Universidade do Porto, Rua Dr. Roberto Frias, 4200-465 Porto, Portugal

A B S T R A C T

This study focuses on bromate (BrO_3^-) removal from pure aqueous solutions by heterogeneous photocatalysis using a stainless steel Kenics® static mixer (SM) as support for the stabilization of TiO_2-P25 thin films. The SM was assembled in a tubular photoreactor coupled to a compound parabolic collector (CPC) for light capture. The effect of the following parameters on the BrO_3^- photocatalytic reduction rate was assessed: SM treatment before TiO_2-P25 deposition, number of TiO_2-P25 layers deposited by dip coating, position of the SM during the coating procedure, solution pH, solution temperature, dissolved oxygen (DO) content, and addition of formic acid (HCOOH) as organic sacrificial agent. Furthermore, the TiO_2-P25 films were characterized and their stability was evaluated. Higher BrO_3^- photocatalytic reduction rates were attained for: the thermally pre-treated SM, 6 TiO_2-P25 layers, the vertically positioned SM during coating, acidic pH, and higher temperatures. The DO had a negligible effect for pH values below 5.5 and a negative effect for higher pH values. The HCOOH declined the BrO_3^- photocatalytic reduction rates when an initial [HCOOH]:[BrO_3^-] molar ratio of 3:1 was applied and had a null influence when used in lower amounts. The generated TiO_2-P25 films proved to be stable.

1. Introduction

Bromine (Br) is abundant in nature mainly in the inorganic form of bromide (Br$^-$). Freshwater can achieve Br$^-$ contents of 15–200 µg L^{-1} [1] as a result of seawater intrusions, connate seawater and anthropogenic sources, such as road salts, fertilizers, coal-fired power plants and textile facilities [2]. Br$^-$ from freshwater can be oxidized to bromate (BrO_3^-) in drinking water treatment plants (DWTP) through disinfection processes such as ozonation, hypochlorination and/or chloramination, with emphasis being placed on the ozonation process [3]. Following ozonation, BrO_3^- concentration in drinking water can range from < 2 to 293 µg L^{-1}, depending on Br$^-$ concentration, ozone dosage, pH, alkalinity and dissolved organic carbon [4]. Based on rodent studies, the International Agency for Research on Cancer classified BrO_3^- as possibly carcinogenic to humans [5]. Consequently, BrO_3^- drinking water standards of 10 µg L^{-1} were implemented by many authorities [6–9]. Moreover, the United States Environmental Protection Agency (US EPA) established a maximum BrO_3^- level goal of zero in drinking water [8].

Techniques to minimize drinking water contamination with BrO_3^- usually fall into three main categories: (i) removal of Br$^-$ prior to BrO_3^- formation, (ii) minimization of BrO_3^- formation during the

ozonation process, and (iii) removal of BrO_3^- from post-ozonation water [10]. The (i) and (ii) approaches typically only result in a partial minimization of BrO_3^- and/or require high operational costs, contrasting with the removal of BrO_3^- after ozonation. Among the various methods for BrO_3^- removal from post-ozonation water, attention should be drawn on heterogeneous photocatalysis due to its improved performance. This advanced reduction process (ARP) is based on the irradiation of a photocatalyst, commonly titanium dioxide (TiO_2), with photons presenting energy equal or greater than its band-gap energy. This promotes the photoexcitation of electrons from the filled valence band (VB) to the empty conduction band (CB), with consequent absorption of these electrons in the CB (e_{CB}^-) and creation of a positive hole in the VB (h_{VB}^+), according to Eq. (1) [11]:

$$TiO_2 + h\nu \rightarrow e_{CB}^- + h_{VB}^+ \tag{1}$$

Two main mechanisms can be considered in the reduction of inorganic compounds M^{n+} by heterogeneous photocatalysis: (i) direct photoreduction by e_{CB}^-, and (ii) indirect photoreduction by strong reducing species (R·) produced by the action of h_{VB}^+ or powerful hydroxyl radicals (HO·) on organic sacrificial agents (OSA) available in the media [12]. Note that HO· are generated via h_{VB}^+ reaction with adsorbed water molecules (H_2O) or hydroxide ions (HO$^-$), according to

---

* Corresponding authors.
  E-mail addresses: francisca.moreira@fe.up.pt (F.C. Moreira), vilar@fe.up.pt (V.J.P. Vilar).

Eqs. (2) and (3) [11]:

$$h_{VB}^+ + H_2O \rightarrow HO^\bullet + H^+ \tag{2}$$

$$h_{VB}^+ + HO^- \rightarrow HO^\bullet \tag{3}$$
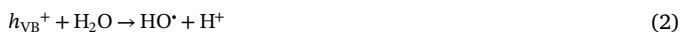
The direct photoreduction by e_{CB}^- occurs via Eq. (4) if inorganic ions have redox potentials that make the reaction thermodynamically possible. In particular, BrO_3^- reduction to Br^- occurs according to Eq. (5) ($E^o = 1.423$ V *vs.* SHE) [13]. For more information on BrO_3^- reduction, the Latimer diagram connecting some Br species for pH < 8.55 can be accessed in Fig. SM-1.

$$M^{n+} + e_{CB}^- \rightarrow M^{(n-1)+} \tag{4}$$

$$BrO_3^- + 6H^+ + 6e^- \rightarrow Br^- + 3H_2O \tag{5}$$
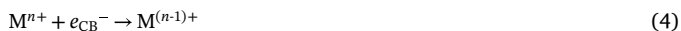
In some cases, the h_{VB}^+ or $HO^\bullet$ can reoxidize the inorganic species to the original oxidation state via Eq. (6), leading to a non-productive short-circuiting of the overall process.

$$M^{(n-1)+} + h_{VB}^+/HO^\bullet \rightarrow M^{n+} \tag{6}$$

In the indirect photoreduction, OSA, commonly carboxylic acids or alcohols, are oxidized by h_{VB}^+ or $HO^\bullet$ via Eq. (7), producing $R^\bullet$.

$$OSA + h_{VB}^+/HO^\bullet \rightarrow R^\bullet + H^+/H_2O \tag{7}$$

$R^\bullet$ can effectively reduce M^{n+}, according to Eq. (8):

$$R^\bullet + M^{n+} \rightarrow R_{ox} + M^{(n-1)+} \tag{8}$$

where R_{ox} can be an aldehyde, a ketone or CO_2, depending on the compound.

For formic acid (HCOOH) and oxalic acid, the strong reducing carbon dioxide radical anion ($CO_2^{\bullet-}$) is formed. For methanol, ethanol and 2-propanolol, 1-hydroxyalkyl radicals are generated. Moreover, the oxidation of OSA by h_{VB}^+ via Eq. (7) can decrease the recombination of e_{CB}^-/h_{VB}^+ pairs and the reoxidation of the inorganic species to the original oxidation state that occurs according to Eq. (6).

The pioneering study on the photocatalytic reduction of BrO_3^- was carried out by Mills et al. [14]. The authors reported the complete removal of 75 μg L^{-1} of BrO_3^- from drinking water after 90 min of reaction using platinized TiO_2-P25 in suspension or after 240 min using platinized TiO_2-P25 immobilized as a thin film on a quartz tube. The platinized TiO_2-P25 film consisted of three TiO_2-P25 layers deposited by pouring an aqueous TiO_2-P25 suspension of 2% (w/v) over the outer wall of the quartz tube, followed by drying, firstly at ambient temperature and secondly at 80 °C for 1 h, and washing with pure water, and further platinized. To our knowledge, this is the only study available on the application of immobilized photocatalysts to BrO_3^- removal from aqueous solutions. All the subsequent researchers who worked on the photocatalytic reduction of BrO_3^- used TiO_2 suspensions, most of them containing commercially available TiO_2 powders [15–19]. Since working with photocatalyst suspensions has significant drawbacks, such as difficult and costly separation of photocatalyst particles from the solution and occurrence of light scattering/absorption [20], the application of immobilized photocatalysts for BrO_3^- reduction should be investigated.

The current work focuses on the photocatalytic reduction of BrO_3^- in pure aqueous solutions using TiO_2-P25 thin films immobilized on an innovative support – a stainless steel Kenics® static mixer (SM). The SM was placed into a borosilicate tubular photoreactor with a compound parabolic collector (CPC) at the bottom for light capture. The current photoreactor design enhances mass transfer due to the intense radial mixing provided by the SM even under laminar flow. The use of laminar flow can minimize the photocatalyst detachment from the support and the energy requirements for pumping the fluid. Furthermore, the entire photocatalyst surface area is illuminated and the radiative transport occurs through the front-side illumination (FSI) mechanism, in which the radiation crosses the fluid and reaches the photocatalyst surface at the fluid/catalyst interface, with consequent generation of the charge carriers (e_{CB}^- and h_{VB}^+) at the fluid/catalyst interface and adjacent area close to the fluid stream. The influence of various operational parameters on the BrO_3^- photocatalytic reduction was assessed. TiO_2 films were characterized and their stability was evaluated.

This study allows to fill the lack of research regarding the use of immobilized photocatalysts for BrO_3^- reduction. Moreover, to the best of our knowledge, this is the first study concerning the use of a SM as catalyst support for the photocatalytic reduction of an inorganic pollutant. The suitability of using a Kenics® SM as support for TiO_2-P25 was already proved by Díez et al. [21] for the oxidation of an organic compound – the antibiotic oxytetracycline (OTC). Dip coating and spray coating techniques were used to immobilize the TiO_2-P25 onto the SM surface and a maximum antibiotic removal of ≈70% after 180 min of reaction (≈4.0 kJ L^{-1} of accumulated ultraviolet (UV) radiation) was achieved applying an initial OTC content of 20 mg L^{-1}.

2. Material and methods

2.1. Chemicals

Sodium bromate > 99% (w/w) purity from Merck was used as BrO_3^- source. Titanium dioxide was Aeroxide® P25 powder (TiO_2-P25) supplied by Evonik and it was used as received. This catalyst exhibited the following characteristics: ≥99.5% (w/w) purity, 80% anatase and 20% rutile crystalline phases, average crystal size of 25 nm, specific surface area of 50 $m^2 g^{-1}$ and density of 3.9 g cm^{-3}. Surfactant Triton™ X-100 was purchased from Sigma-Aldrich. Formic acid was 99.5% (w/w) purity from VWR. Sodium bromide > 99% (w/w) purity from Merck was applied as Br^- source. Alkaline detergent was Derquim LM 01 from Panreac. Sulfuric acid 95% (w/w) purity from Fisher Scientific was applied in the SM chemical treatment. Hydrochloric acid 37% (w/w) purity from Fisher Scientific and sodium hydroxide ≥99% (w/w) from Labkem were used in pH adjustments. Standards for ion chromatography were purchased from Sigma-Aldrich and Fluka. Potassium hydroxide applied as eluent in ion chromatography was supplied from Thermo Fisher Scientific. Ultrapure water used as matrix and in analyses was obtained from a Millipore® Direct-Q system (18.2 MΩ cm resistivity at 25 °C).

2.2. Experimental system

The experimental system was mainly composed of: (i) a 0.271 L capacity jets photoreactor comprising a borosilicate tube filled with a Kenics® SM, exhibiting polypropylene (PP) caps at the tube ends and coupled to a CPC at the bottom for light capture, (ii) a solar radiation simulator (Atlas, model Suntest XLS+) equipped at the top with a 1700 W air-cooled xenon arc lamp emitting radiation from 280 to 800 nm, set at 500 W m^{-2} and giving a radiant power of 0.61 ± 0.02 W from 280 to 405 nm in the system that provides an accumulation of 1.5–1.6 kJ L^{-1} per hour for 1.50-1.38 L of solution, and (iii) a 1.6 L capacity recirculation cylindrical glass vessel thermostatically controlled and magnetically stirred. All the system units were connected by polytetrafluoroethylene (PTFE) tubing. Díez et al. [21] displays a detailed description of the system and its sketch. The Kenics® SM was made of 304 stainless steel (66–74% of iron, 18–20% of chromium and 8–10% of nickel, among other minor constituents) and consisted of two helical mixing elements, each one with 4.5 cm height, 9.8 cm length and 0.35 cm thickness, providing a total volume of 31 cm^3 and a total surface area of 190 cm^2. The CPC consisted of two reflectors in the shape of a truncated parabola made of uncoated anodized aluminum (R85). It promoted the illumination of the entire photoreactor perimeter, which resulted in an illuminated catalyst surface area per unit of reactor volume of 79 $m^2 m^{-3}$. A radiant power of 0.61 ± 0.02 W from 280 to 405 nm was reaching the system, as determined in Díez et al. [21] using 2.5 mmol L^{-1} of 2-nitrobenzaldehyde actinometer.

The experimental procedure can be accessed in the Supplementary Material file. The same TiO$_2$-P25 film was applied in various consecutive trials. A known reaction was carried out every four consecutive trials employing the same TiO$_2$-P25 film to assess the integrity of the film.

2.3. Preparation of the SM before photocatalyst films deposition

The commercial stainless steel Kenics® SM was subjected to: (i) sandblast abrasion, (ii) impurities removal, and (iii) thermal treatment or thermal treatment followed by chemical treatment. Sandblast abrasion was performed in a wet sandblasting cabinet. The procedure for impurities removal was the following: (i) immersion of the SM in an alkaline detergent solution and provision of sonication at 37 kHz for 15 min by an ultrasonic bath Elmasonic S 120 (H) from Elma, (ii) rinsing with ultrapure water in abundance, and (iii) drying at room temperature. Thermal and chemical treatments were based on Rodriguez et al. [22] procedure. The thermal treatment was carried out in a furnace using a temperature ramp rate of 2 °C min^{-1} until 500 °C and maintaining this temperature for 4 h. Afterwards, the furnace was cooled down up to reach room temperature. The chemical treatment was performed by immersing the SM in a sulfuric acid solution of 10% (w/w) for 3 h. Afterwards, the SM was: (i) rinsed with ultrapure water in abundance, (ii) immersed two times in ultrapure water under sonication at 37 kHz for 30 min, and (iii) dried at 100 °C for 1 h.

2.4. Photocatalyst films preparation and characterization

A TiO$_2$-P25 aqueous suspension of 2% (w/v) was prepared using ultrapure water and adding 1 drop of Triton™ X-100 per 100 mL of solution. Immediately before use, this suspension was sonicated for 15 min in an ultrasonic processor Vibra-Cell™ VCX 130 from Sonics at 20 kHz (80% amplitude) to better disperse particles. An automatic dip coating unit RDC 15 from Bungard-Elektronik was employed using a speed of insertion and drawing of 50 mm min^{-1} and a dipping time of 30 s. The SM was drowned into the TiO$_2$-P25 aqueous suspension either vertically or horizontally. All the SM surface area was coated. Different number of photocatalyst layers were deposited on the SM surface by varying the number of dips (1, 3, 6 and 12). After the deposition of each layer, the SM was dried at room temperature for ca. 3 min and at 60 °C for 30 min. Before the use of the coated SM in photocatalytic trials, this device was placed inside the borosilicate tube and ultrapure water was recirculated throughout the system in the dark for 3 h to remove some unattached TiO$_2$-P25 particles.

Morphology of stainless steel SM surface and TiO$_2$-P25 films was determined by scanning electron microscopy (SEM) using electron backscatter diffraction (EBSD) technique and energy dispersive X-ray (EDS) analysis. A FEI Quanta 400 FEG ESEM/EDAX Genesis X4 M apparatus equipped with a Schottky field emission gun (for optimal spatial resolution) was employed. To get coated samples for analysis, various 1 cm^2 pieces of 304 stainless steel were attached to the SM in different locations before pre-treatments and coating procedures. For SEM analysis, the coated samples were mounted on a carbon double-sided adhesive tape and analyzed at different magnifications.

The stability of the various photocatalyst films under different experimental conditions was always assessed by performing each experiment in triplicate. The average values were presented along this study. Moreover, twenty-five consecutive trials were performed employing the photocatalyst film resulting from the deposition of 6 TiO$_2$-P25 layers on the vertically assembled and previously thermally treated SM. An ultrasound test was also carried out, based on changes in the BrO$_3^-$ photocatalytic reduction rate after subjecting the previously mentioned SM to sonication. In this test, the SM was immersed into a 1 L beaker containing ultrapure water and sonicated for a total of 60 min at 37 kHz.

2.5. Analytical determinations

The concentration of BrO$_3^-$, Br$^-$ and HCOOH was followed by ion chromatography by injecting 5 μL samples into a Dionex ICS-2100 liquid chromatograph equipped with (i) a Dionex IonPac AG19 (2 × 50 mm) + IonPac AS19 (2 × 250 mm) column at 30 °C, and (ii) a Dionex Anion Electrolytically Regenerated Suppressor 500 (2 mm) in Auto Suppression Recycle Mode and with the application of a current of 15 mA. Isocratic elution of 20 mM potassium hydroxide at a flow rate of 0.30 mL min^{-1} was applied. Retention times for HCOOH (formate ion – HCOO$^-$ – at the eluent pH), BrO$_3^-$ and Br$^-$ were around 3.6 min, 4.0 min and 6.2 min, respectively. Limits of quantification and detection were: 0.14 μM and 0.05 μM, respectively, for BrO$_3^-$ and Br$^-$, and 0.23 μM and 0.10 μM, respectively, for HCOOH. Solution pH and temperature were determined by an inoLab 730 laboratory meter from WTW. DO was determined by a HI 98,194 multiparameter analyzer from HANNA Instruments. Before ion chromatography analysis, samples were filtered with 0.20 μm Nylon filters from Whatman.

2.6. Pseudo-first-order kinetic fitting

The pseudo-first-order kinetic constants for BrO$_3^-$ reduction ($k_{bromate}$), in min^{-1}, were determined according to the procedure presented in the Supplementary Material file. Table 1 exhibits the $k_{bromate}$ values for the various experiments within this study.

2.7. Calculations on the position of CB and VB edges for TiO$_2$-P25 and on the redox potential of species in solution at different pH values

Calculations were carried out considering that the potential determining ions on the TiO$_2$/electrolyte solution interface were the HO$^-$ and H$^+$ provided by the water in solution [23]. The Nernst equation was applied in all calculations. CB and VB edges for TiO$_2$-P25 were given by Martin et al. [24]. Standard redox potentials for the various redox pairs were given by Lide [13] and Armstrong et al. [25].

3. Results and discussion

3.1. General considerations

Concentrations of BrO$_3^-$, Br$^-$, HCOOH and DO were given in μM throughout this study in order to better assess the conversion of BrO$_3^-$ into Br$^-$ and the ratios of HCOOH and DO to BrO$_3^-$.

A flow rate of 50 L h^{-1} (Reynolds number of 380; laminar flow) was applied in all trials since this flow rate was selected as optimum for the current experimental system by Díez et al. [21]. A pH of 5.5 was selected for some trials because Zhang et al. [16] achieved the fastest BrO$_3^-$ photocatalytic reduction rates at this pH using suspensions of TiO$_2$-P25.

Photolysis of BrO$_3^-$ in the absence of the SM at pH 5.5 provided negligible BrO$_3^-$ reductions after 180 min. In the presence of HCOOH, photolysis experiments also provided negligible BrO$_3^-$ reductions at solution pH of 5.5 or 6.5 and [HCOOH]:[BrO$_3^-$] molar ratios from 0.5:1 to 3:1. The HCOOH only absorbs radiation for wavelengths below ca. 250 nm, and thus the radiation emitted by the xenon lamp (wavelengths above 280 nm) was unable to provide HCOOH photolysis. Dark experiments (catalysis) revealed negligible BrO$_3^-$ adsorption on the TiO$_2$-P25 surface for different number of photocatalyst layers and pH values. Dark experiments employing HCOOH are discussed in Section 3.8.

Using 1.56 μM of Br$^-$ as starting compound, a constant Br$^-$ content was detected along with null BrO$_3^-$ contents for photocatalytic trials at pH from 3.0 to 7.0. This can be attributed to a low reaction rate between Br$^-$ and h_{VB}^+ or HO$^·$ and/or to a fast reduction of formed BrO$_3^-$ to Br$^-$ by the available e_{CB}^-.

For all trials carried out within this study, the rate of disappearance of BrO$_3^-$ ions was similar to the rate of formation of Br$^-$ ions, with no identification of by-products.

Table 1

$k_{bromate}$ values along with the corresponding time interval of adjustment, residual variance (S_R^2) and coefficient of determination (R^2).

System			Time interval (min)	$k_{bromate}$ (10^{-3} min^{-1})	S_R^2 (μM^2)	R^2
Influence of SM pre-treatment[5]	SA[1] + IR[2] + TT[3]		0–180	7.19 ± 0.07	1.1×10^{-3}	0.999
	SA[1] + IR[2] + TT[3] + CT[4]		0–180	4.81 ± 0.06	1.2×10^{-3}	0.998
Influence of number of photocatalyst layers[6]	1 layer		0–180	5.07 ± 0.04	5.3×10^{-4}	0.999
	3 layers		0–180	7.19 ± 0.07	1.1×10^{-3}	0.999
	6 layers		0–180	8.90 ± 0.07	7.3×10^{-4}	1.00
	12 layers		0–180	8.8 ± 0.1	1.9×10^{-3}	0.999
Influence of SM position during dip coating[7]	Vertical		0–180	8.90 ± 0.07	7.3×10^{-4}	1.00
	Horizontal		0–180	5.5 ± 0.2	7.6×10^{-3}	0.991
Influence of solution pH[8]	3.0		0–150	17.3 ± 0.8	1.5×10^{-2}	0.992
	4.0		0–150	17.6 ± 0.8	2.0×10^{-2}	0.992
	5.5		0–180	8.90 ± 0.07	7.3×10^{-4}	1.00
	6.5		0–180	1.95 ± 0.04	1.6×10^{-3}	0.992
	7.0		0–180	1.22 ± 0.02	6.1×10^{-4}	0.992
Influence of solution temperature[9]	15 °C		0–180	6.4 ± 0.2	6.7×10^{-3}	0.994
	20 °C		0–180	7.5 ± 0.2	5.8×10^{-3}	0.996
	25 °C		0–180	8.90 ± 0.07	7.3×10^{-4}	1.00
	30 °C		0–180	9.6 ± 0.1	1.6×10^{-3}	0.999
Influence of DO content[10]	pH 3.0	[DO]: 212–239 µM	0–150	17.3 ± 0.8	1.5×10^{-2}	0.992
		[DO]: < 3.1 µM	0–150	17.3 ± 0.9	1.9×10^{-2}	0.991
	pH 4.0	[DO]: 212–239 µM	0–150	17.6 ± 0.8	2.0×10^{-2}	0.992
		[DO]: < 3.1 µM	0–150	16.6 ± 0.9	2.0×10^{-2}	0.990
	pH 5.5	[DO]: 212k239 µM	0–180	8.90 ± 0.07	7.3×10^{-4}	1.00
		[DO]: < 3.1 µM	0–180	8.7 ± 0.1	1.6×10^{-3}	0.999
	pH 6.5	[DO]: 212–239 µM	0–180	1.95 ± 0.04	1.6×10^{-3}	0.992
		[DO]: < 3.1 µM	0–180	3.35 ± 0.08	4.0×10^{-3}	0.992
	pH 7.0	[DO]: 212-239 µM	0–180	1.22 ± 0.02	6.1×10^{-4}	0.992
		[DO]: < 3.1 µM	0–180	1.60 ± 0.04	1.3×10^{-3}	0.991
Influence of addition of HCOOH as OSA[11]	pH 6.5, [DO]: 212-239 µM	Absence of HCOOH	0–180	1.95 ± 0.04	1.6×10^{-3}	0.992
		[HCOOH]:[BrO$_3^-$] molar ratio: 0.5:1	0–180	2.10 ± 0.05	2.1×10^{-3}	0.991
		[HCOOH]:[BrO$_3^-$] molar ratio: 1:1	0–180	2.02 ± 0.04	1.4×10^{-3}	0.994
		[HCOOH]:[BrO$_3^-$] molar ratio: 3:1	0–180	1.30 ± 0.05	2.1×10^{-3}	0.980
	pH 6.5, [DO]: < 3.1 µM	Absence of HCOOH	0–180	3.35 ± 0.08	4.0×10^{-3}	0.992
		[HCOOH]:[BrO$_3^-$] molar ratio: 0.5:1	0–180	3.60 ± 0.07	2.6×10^{-3}	0.995
		[HCOOH]:[BrO$_3^-$] molar ratio: 1:1	0–180	3.22 ± 0.08	4.0×10^{-3}	0.992
		[HCOOH]:[BrO$_3^-$] molar ratio: 3:1	0–180	2.27 ± 0.04	1.2×10^{-3}	0.996
	pH 5.5, [DO]: 212-239 µM	Absence of HCOOH	0–180	8.90 ± 0.07	7.3×10^{-4}	1.00
		[HCOOH]:[BrO$_3^-$] molar ratio: 1:1	0–180	9.0 ± 0.2	3.2×10^{-3}	0.998
Stability of photocatalyst films - Ultrasound test[12]	Before SM sonication		0–180	8.90 ± 0.07	7.3×10^{-4}	1.00
	After SM sonication for 60 min		0–180	6.2 ± 0.3	1.6×10^{-2}	0.981

[1] SA: Sandblast abrasion.

[2] IR: Impurities removal.

[3] TT: Thermal treatment.

[4] CT: Chemical treatment.

[5] Conditions: [BrO$_3^-$]$_0$: 1.56 µM; SM position during dip coating: vertical; Number of photocatalyst layers: 3; Solution pH: 5.5; Solution temperature: 25 °C; [DO]: 212–239 µM.

[6] Conditions: [BrO$_3^-$]$_0$: 1.56 µM; SM pre-treatment: SA[1] + IR[2] + TT[3]; SM position during dip coating: vertical; Solution pH: 5.5; Solution temperature: 25 °C; [DO]: 212–239 µM.

[7] Conditions: [BrO$_3^-$]$_0$: 1.56 µM; SM pre-treatment: SA[1] + IR[2] + TT[3]; Number of photocatalyst layers: 6; Solution pH: 5.5; Solution temperature: 25 °C; [DO]: 212–239 µM.

[8] Conditions: [BrO$_3^-$]$_0$: 1.56 µM; SM pre-treatment: SA[1] + IR[2] + TT[3]; SM position during dip coating: vertical; Number of photocatalyst layers: 6; Solution temperature: 25 °C; [DO]: 212–239 µM.

[9] Conditions: [BrO$_3^-$]$_0$: 1.56 µM; SM pre-treatment: SA[1] + IR[2] + TT[3]; SM position during dip coating: vertical; Number of photocatalyst layers: 6; Solution pH: 5.5; [DO]: 212–239 µM.

[10] Conditions: [BrO$_3^-$]$_0$: 1.56 µM; SM pre-treatment: SA[1] + IR[2] + TT[3]; SM position during dip coating: vertical; Number of photocatalyst layers: 6; Solution temperature: 25 °C.

[11] Conditions: [BrO$_3^-$]$_0$: 1.56 µM; SM pre-treatment: SA[1] + IR[2] + TT[3]; SM position during dip coating: vertical; Number of photocatalyst layers: 6; Solution temperature: 25 °C.

[12] Conditions: [BrO$_3^-$]$_0$: 1.56 µM; SM pre-treatment: SA[1] + IR[2] + TT[3]; SM position during dip coating: vertical; Number of photocatalyst layers: 6; Solution pH: 5.5; Solution temperature: 25 °C; [DO]: 212–239 µM.

3.2. Influence of SM pre-treatment

SM pre-treatment was carried out to increase the SM surface roughness at macro, micro and nanoscale levels, thereby enhancing the attachment of TiO_2-P25 particles to the SM surface. The SM was firstly subjected to sandblast abrasion to create some macroroughness in its surface since it was made of plain polished stainless steel (Fig. 1). SM roughness was highly improved by this treatment as clearly visible to the human eye (Fig. 1). Afterwards, potential small impurities resulting from the abrasion procedure and SM handling were removed by ultrasonically cleaning the SM in an alkaline detergent solution followed by rinsing with ultrapure water and drying at ambient temperature. No visible changes in the SM were observed after impurities removal. Finally, the SM underwent thermal treatment or thermal treatment followed by chemical treatment with sulfuric acid. The thermal treatment made the SM surface darker (Fig. 1) and SEM analysis revealed a high surface roughness at the microscale level (Fig. 2). Subsequent sulfuric acid attack made the SM visibly blurred (Fig. 1) and SEM images
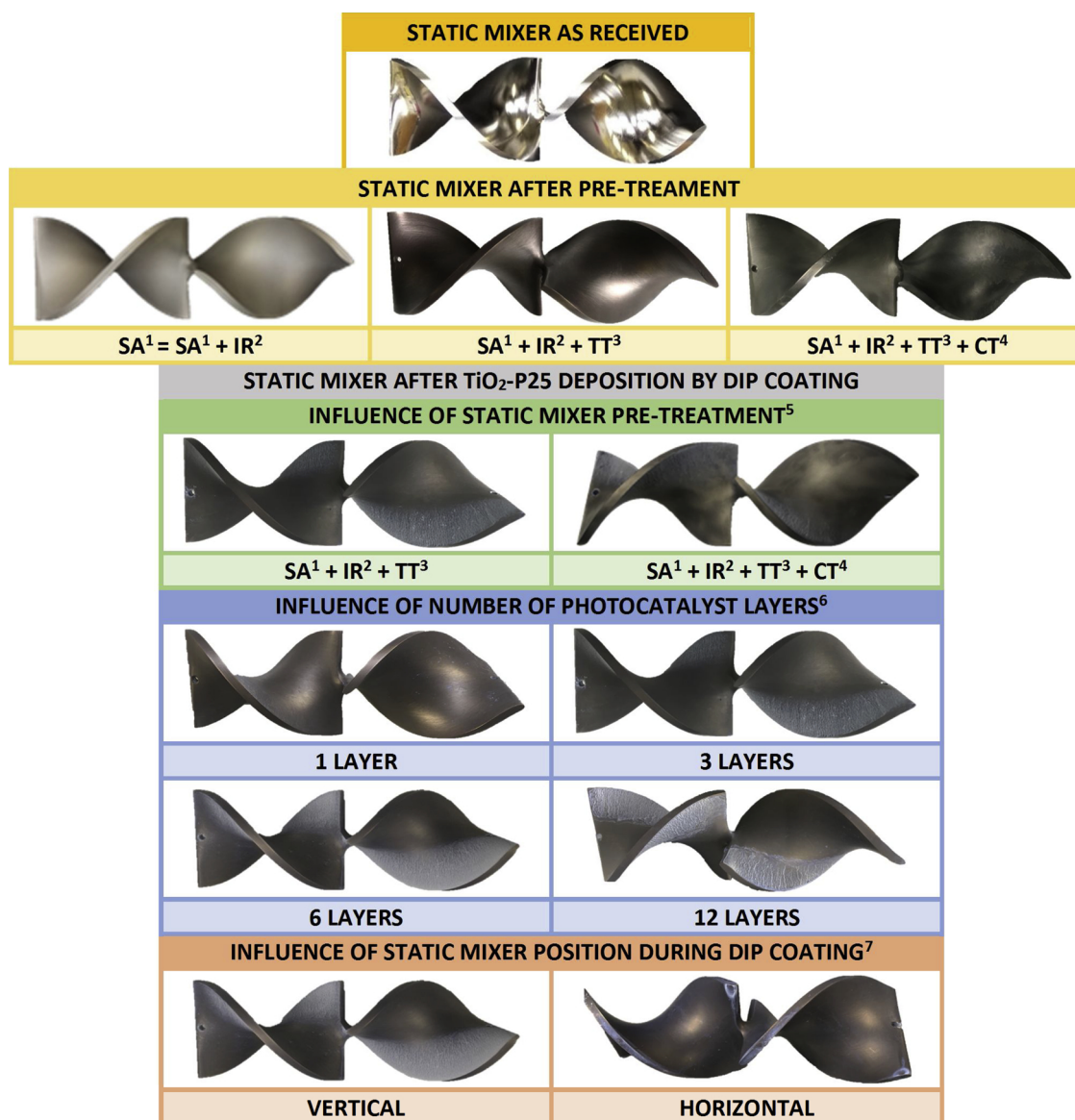
STATIC MIXER AS RECEIVED

STATIC MIXER AFTER PRE-TREAMENT

| $SA^1 = SA^1 + IR^2$ | $SA^1 + IR^2 + TT^3$ | $SA^1 + IR^2 + TT^3 + CT^4$ |

STATIC MIXER AFTER TiO$_2$-P25 DEPOSITION BY DIP COATING

INFLUENCE OF STATIC MIXER PRE-TREATMENT^5

| $SA^1 + IR^2 + TT^3$ | $SA^1 + IR^2 + TT^3 + CT^4$ |

INFLUENCE OF NUMBER OF PHOTOCATALYST LAYERS^6

| 1 LAYER | 3 LAYERS |
| 6 LAYERS | 12 LAYERS |

INFLUENCE OF STATIC MIXER POSITION DURING DIP COATING^7

| VERTICAL | HORIZONTAL |

^{1}**SA: Sandblast abrasion;**
^{2}**IR: Impurities removal;**
^{3}**TT: Thermal treatment;**
^{4}**CT: Chemical treatment;**
^{5}**Conditions: SM position during dip coating: vertical; Number of photocatalyst layers: 3;**
^{6}**Conditions: SM pre-treatment: SA^1 + IR^2 + TT^3; SM position during dip coating: vertical;**
^{7}**Conditions: SM pre-treatment: SA^1 + IR^2 + TT^3; Number of photocatalyst layers: 6.**

**Fig. 1.** Photos of the SM in different stages.

disclose a high enhancement of roughness at the nanoscale level (Fig. 2). It is worth mentioning that the SM acquired a very dark brownish grey color in the course of the sulfuric acid attack, later removed by water rising. This can be attributed to the dissolution of iron and chromium (the main components of stainless steel) by the acid, with consequent restructuration of the stainless steel surface [26].

TiO$_2$-P25 films were deposited on the SM surface subjected either to thermal or thermal/chemical treatment. The thermally pre-treated SM displayed an accumulation of higher amounts of TiO$_2$-P25 particles along the edges, as can be seen in Fig. 1. This was confirmed by SEM images (Fig. 2), which exhibit lighter grey areas in the center and darker grey areas in the edges, for which EDS analysis confirmed the presence of higher TiO$_2$ contents. This non-uniform TiO$_2$-P25 particles distribution was much less pronounced for the thermally/chemically pre-treated SM (Figs. 1 and 2). Nevertheless, the mechanical stabilization of TiO$_2$-P25 in

the thermally/chemically treated SM was only good for fine particles due to the high surface roughness at the nanoscale level (Fig. 2). In contrast, a good stabilization of both fine TiO$_2$-P25 particles and large powder agglomerates occurred for the thermally treated SM in virtue of its higher roughness at larger scale (Fig. 2). Fig. 3a shows a higher BrO$_3^-$ photocatalytic reduction rate for the thermally pre-treated SM compared to the thermally/chemically pre-treated device ($k_{bromate}$ variation by 33% – Table 1), which indicates a high participation of the larger powder agglomerates immobilized on the thermally pre-treated SM surface in the BrO$_3^-$ photocatalytic reduction.

3.3. Influence of number of photocatalyst layers

The generation of thicker TiO$_2$-P25 films for increasing number of deposited photocatalyst layers was perceptible to the naked eye (Fig. 1).
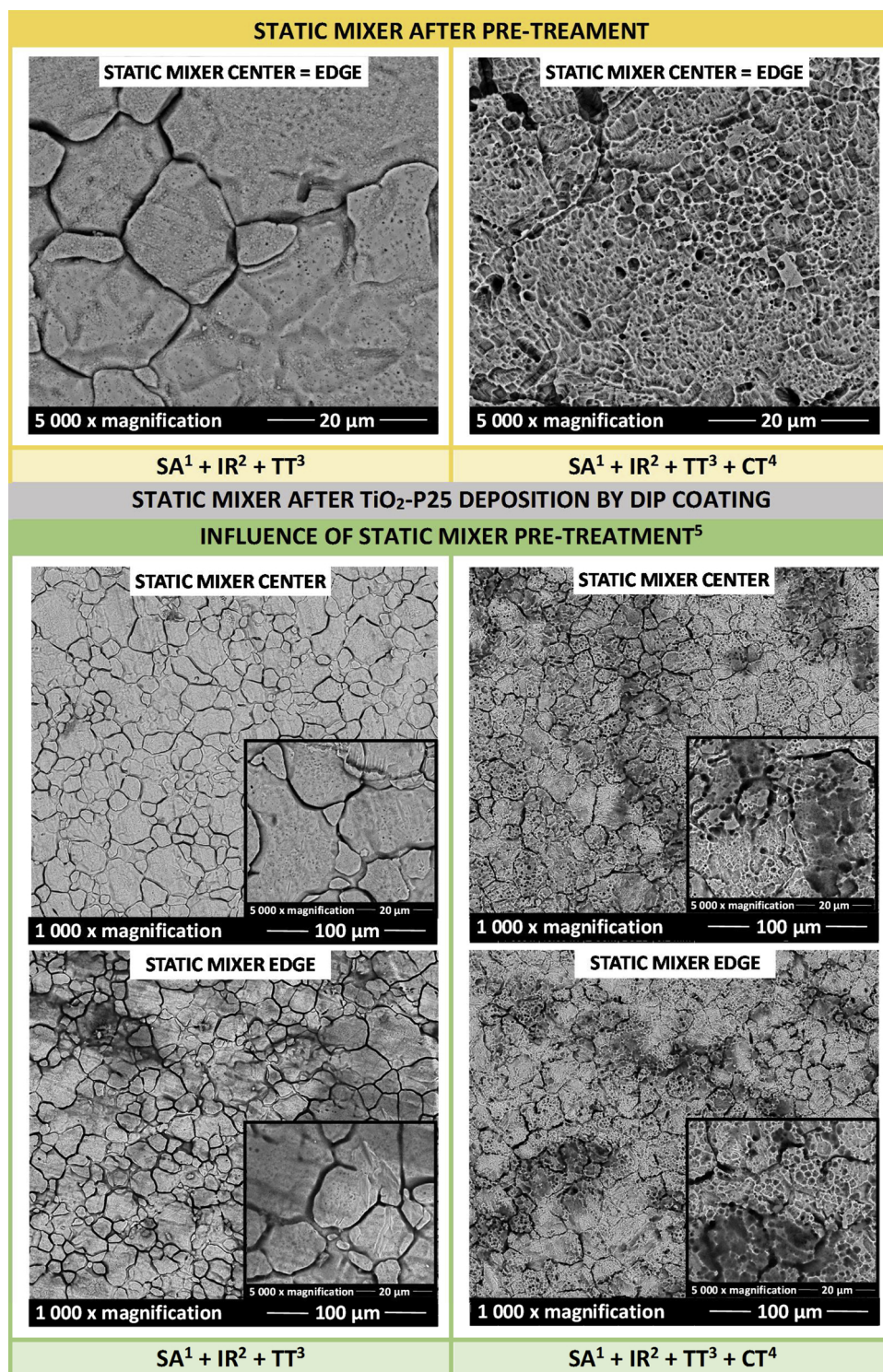
Fig. 2. SEM images of the SM after pre-treatment and of the TiO$_2$-P25 films deposited on the SM surface subjected to different pre-treatments.

In the SEM micrographs (Fig. SM-2), the higher amount of TiO$_2$-P25 for increasing number of layers is given by the occurrence of darker grey regions.

In terms of BrO$_3^-$ photocatalytic reduction rates, Fig. 3b shows higher rates for increasing number of TiO$_2$-P25 layers up to 6, which corresponds to an average film thickness of 700 nm, and similar rates for 6 and 12 photocatalyst layers. The $k_{bromate}$ varied by ca. 43% from 1 layer to 6/12 layers (Table 1). These results can be attributed to an increase in the available area for the production of charge carriers (e_{CB}^- and h_{VB}^+) for thicker TiO$_2$-P25 films together with the capability
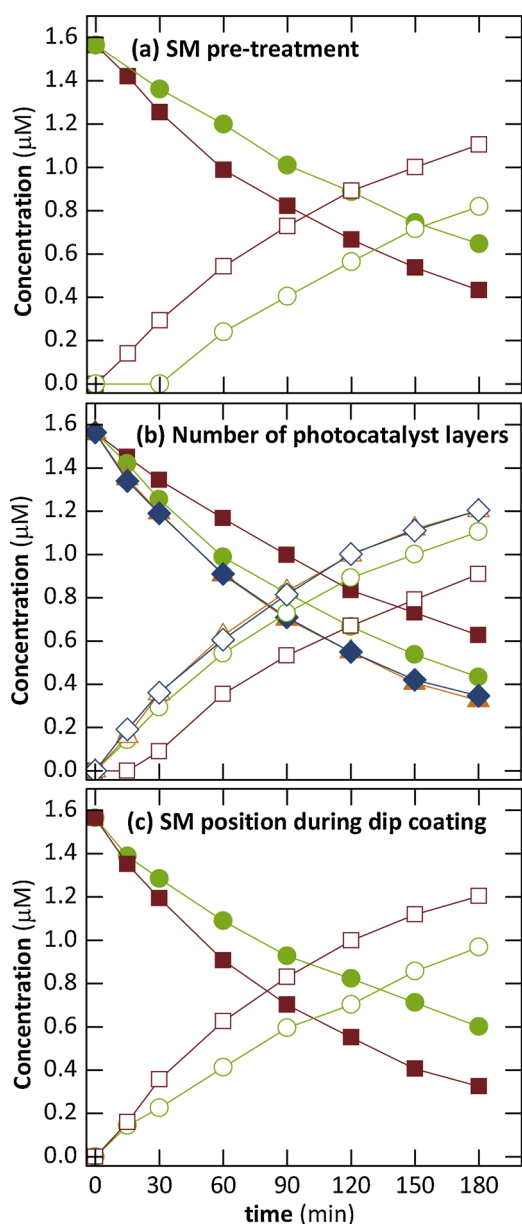
Fig. 3. Influence of SM pre-treatment (a), number of photocatalyst layers (b) and SM position during dip coating (c) on BrO_3^- photocatalytic reduction. Solid symbols: BrO_3^-. Open symbols: Br^-. SM pre-treatment: $SA^1 + IR^2 + TT^3$ (■,□), $SA^1 + IR^2 + TT^3 + CT^4$ (●,○) (conditions: SM position during dip coating: vertical; Number of photocatalyst layers: 3). Number of photocatalyst layers: 1 (■,□), 3 (●,○), 6 (▲,△), 12 (◆,◇) (conditions: SM pre-treatment: $SA^1 + IR^2 + TT^3$; SM position during dip coating: vertical). SM position during dip coating: vertical (■,□), horizontal (●,○) (conditions: SM pre-treatment: $SA^1 + IR^2 + TT^3$; Number of photocatalyst layers: 6). General conditions: $[BrO_3^-]_0$: 1.56 μM; Solution pH: 5.5; Solution temperature: 25 °C; [DO]: 212–239 μM. [1]SA: Sandblast abrasion; [2]IR: Impurities removal; [3]TT: Thermal treatment; [4]CT: Chemical treatment.

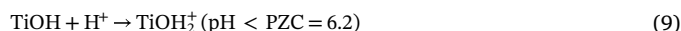of UV light and reactants to only penetrate/diffuse within a specific film thickness.

3.4. Influence of SM position during dip coating

For the horizontally assembled SM during dip coating, the TiO_2-P25 particles were equally distributed along the SM edges and center, in contrast to the dissimilarities obtained for the vertically positioned SM. Naked eye observations (Fig. 1) and microscale images (Fig. SM-3)

support this outcome. Moreover, the number of TiO_2-P25 particles agglomerates (dark grey circles detected by SEM) was much lower for the horizontally mounted SM, especially when compared to the edges of the vertically assembled SM. The spiral shape of the SM may have contributed to these distinct powder distributions. Fig. 3c shows a higher BrO_3^- removal rate for the application of the SM in the vertical position ($k_{bromate}$ variation by 38% – Table 1). This indicates that the higher amount of TiO_2-P25 particles deposited on the edges of the vertically mounted SM has an important role in the BrO_3^- photocatalytic reduction. Stability of these non-uniform photocatalyst films is discussed in Section 3.9.

3.5. Influence of solution pH

Fig. 4a displays higher BrO_3^- photocatalytic reduction rates for more acidic pH values from 7.0 to 4.0 ($k_{bromate}$ variation by 93% – Table 1) along with quite similar rates for pH 3.0 and 4.0. These results can be mainly attributed to a growing electrostatic attraction between TiO_2-P25 and BrO_3^- for more acidic pH values under the point of zero charge (PZC) of TiO_2-P25 – pH ca. 6.2 [27] – together with a rising electrostatic repulsion between TiO_2-P25 and BrO_3^- for increasing pH values above 6.2, taking into account the occurrence of Eqs. (9) and (10).

$$TiOH + H^+ \rightarrow TiOH_2^+ \, (pH < PZC = 6.2) \tag{9}$$

$$TiOH + HO^- \rightarrow TiO^- + H_2O \, (pH > PZC = 6.2) \tag{10}$$

The quite similar BrO_3^- removal at pH 3.0 and 4.0 suggests a quite similar driving force of BrO_3^- to the TiO_2-P25 surface.

In addition, BrO_3^- reduction is favored at more acidic pH values according to Eq. (5).

The pH also affects the TiO_2-P25 band edge positions and the redox potential of the Br^-/BrO_3^- pair and of other reactants, including H_2O/O_2, H^+/H_2, $O_2^{\cdot-}/O_2$, $H_2O/HO^{\cdot}$ and $CO_2^{\cdot-}/CO_2$ pairs. Fig. 4a_1 reveals a Nernstian shift of the TiO_2-P25 band edge positions with pH, yielding a change of -0.059 V per pH unit. This would lead to a higher reductive power for higher pH values if the redox potential of the Br^-/BrO_3^- pair was independent of the pH value. However, the Br^-/BrO_3^- pair redox potential exhibits a similar Nernstian pH dependence, as well as all the other above-mentioned reactants (Fig. 4a_1), which points to similar potential differences between the Br^-/BrO_3^- pair and all the reducing agents for all pH values.

Studies using photocatalyst suspensions also found higher BrO_3^- photocatalytic reduction rates for lower pH values, namely Lin et al. [28], which applied TiO_2-P25 as photocatalyst in the presence of methanol and a pH range of 3–11, Noguchi et al. [19], where TiO_2-ST-21 (anatase) was employed together with a pH range of 5–7, and Zhang et al. [29], which used graphene oxide and fluorine co-doped TiO_2 and a pH range of 3.13-9.08.
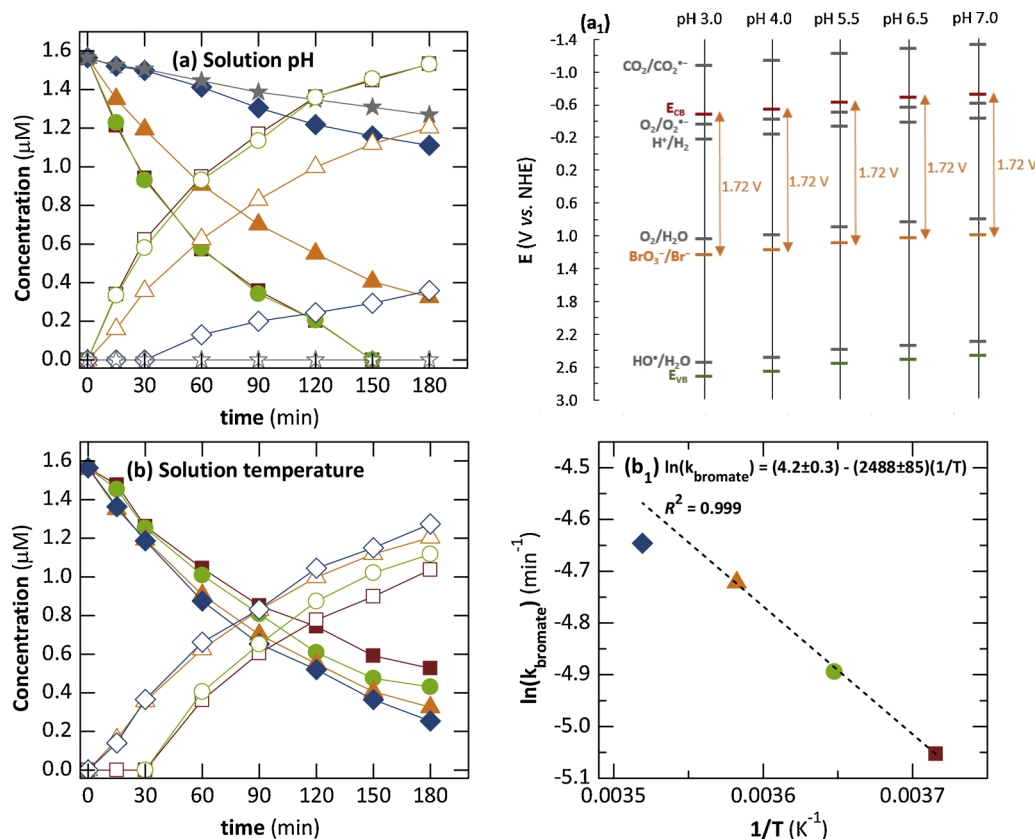
3.6. Influence of solution temperature

Fig. 4b shows increasing BrO_3^- photocatalytic reduction rates for increasing temperatures from 15 °C to 30 °C ($k_{bromate}$ variation of 33% – Table 1). However, this positive effect of temperature was less pronounced from 25 °C to 30 °C. The increase of $k_{bromate}$ with increasing temperature from 15 °C to 25 °C can be entirely attributed to the Arrhenius Eq. (11) [30], as demonstrated by the perfect correlation of $k_{bromate}$ and temperature data in Fig. 4b_1 ($R^2 = 0.999$).

$$\ln(k_{bromate}) = \ln(A) - \frac{E_a}{R}\frac{1}{T} \tag{11}$$

where A is the pre-exponential factor (min^{-1}), E_a is the activation energy (J mol^{-1}), R is the universal gas constant (8.314 J mol^{-1} K^{-1}), and T is the solution absolute temperature (K).

For 30 °C, the $k_{bromate}$ value was below the expected value according

Fig. 4. Influence of solution pH (a) and solution temperature (b) on BrO_3^- photocatalytic reduction. Solid symbols: BrO_3^-. Open symbols: Br^-. Solution pH: 3.0 (■,□), 4.0 (●,○), 5.5 (▲,△), 6.5 (◆,◇), 7.0 (★,☆) (conditions: Solution temperature: 25 °C). Solution temperature: 15 °C (■,□), 20 °C (●,○), 25 °C (▲,△), 30 °C (◆,◇) (conditions: Solution pH: 5.5). General conditions: $[BrO_3^-]_0$: 1.56 μM; SM pretreatment: SA[1] + IR[2] + TT[3]; SM position during dip coating: vertical; Number of photocatalyst layers: 6, [DO]: 212–239 μM. [1]SA: Sandblast abrasion; [2]IR: Impurities removal; [3]TT: Thermal treatment. Fig. 4a[1] displays the effect of pH on the position of CB and VB edges for TiO_2-P25 and on the redox potential of Br^-/BrO_3^-, H_2O/O_2, H^+/H_2, $O_2^{·-}/O_2$, $H_2O/HO^·$ and $CO_2^{·-}/CO_2$ pairs at 25 °C. Fig. 4b[1] displays the Arrhenius plot of influence of temperature data.

to the Arrhenius equation (11) (Fig. 4b[1]). This suggests the occurrence of weaker adsorption of reactants to the TiO_2-P25 surface and/or faster recombination of e_{CB}^-/h_{VB}^+ pairs due to thermal agitation [11] for temperatures above 25 °C.

The current achievements contrast with the ones found in Lin et al. [28] for BrO_3^- removal using TiO_2-P25 in suspension and in the presence of methanol, where $k_{bromate}$ was accelerated for increasing temperatures from 20 °C to 60 °C.

Note that higher temperatures can also diminish O_2 solubility in water, which can affect the photocatalytic reduction of inorganic species, as discussed in Section 3.7. Nevertheless, the influence of DO on the BrO_3^- photocatalytic reduction was negligible at pH 5.5 (see detailed discussion in Section 3.7), thereby not affecting the current trials.

It should also be noted that the potential difference between TiO_2-P25 band edge positions and redox potential of Br^-/BrO_3^- pair and of other reactants was similar for all temperatures since all these variables displayed a Nernstian temperature dependence.

3.7. Influence of DO content

Conventional experiments, in which the aqueous solution was in contact with the atmosphere, registered DO contents of 212–239 μM. Trials with DO contents below the detection limit of the DO analyzer, i.e., 3.1 μM, were also performed by purging DO with the injection of nitrogen gas (N_2). It is worth mentioning that DO contents capable of affecting the reactions may have been available in all or some of the experiments with the provision of N_2 since the detection limit of the DO analyzer (3.1 μM) was approximately twice the initial molar content of BrO_3^- (1.56 μM).

The influence of DO content on the BrO_3^- photocatalytic reduction rate was assessed for various solution pH values. Fig. 5 shows a negligible influence of DO for acidic pH values of 3.0, 4.0 and 5.5, and a negative effect for pH 6.5 ($k_{bromate}$ decreased by 42% - Table 1) and pH 7.0 ($k_{bromate}$ decreased by 24% - Table 1). The results at pH 3.0, 4.0 and

5.5 can be attributed to one of the two following mechanisms: (i) absence of DO reaction with e_{CB}^- via Eq. (12) [11] in virtue of the strong electrostatic attraction between BrO_3^- and TiO_2-P25 that takes place for pH values below 6.2 (PZC of TiO_2-P25), or (ii) occurrence of Eq. (12), with consequent decrease of BrO_3^- reduction rate, counterbalanced by the improvement of BrO_3^- reduction rate due to the acting of some DO reduction products as mediators for BrO_3^- reduction. These mediators include the superoxide anion radical ($O_2^{·-}$), i.e., the primary product of DO reduction by e_{CB}^- via Eq. (12), and hydrogen peroxide (H_2O_2), which is generated from the protonation of $O_2^{·-}$ via Eq. (13) followed by Eq. (14) [11].

$$O_2 + e_{CB}^- \rightarrow O_2^{·-} \tag{12}$$

$$O_2^{·-} + H^+ \rightarrow HOO^· \tag{13}$$

$$2HOO^· \rightarrow H_2O_2 + O_2 \tag{14}$$

Zhang et al. [16] even reported a decrease in the $k_{bromate}$ by 39% at pH 5.5 for trials in the absence of DO compared to air-atmospheric trials when applying TiO_2-P25 suspensions. The authors attributed these results to the presence of higher amounts of H_2O_2 for trials in the presence of DO.

The negative effect of DO for pH 6.5 and 7.0 can be ascribed to the occurrence in high extent of the scavenging of e_{CB}^- by DO via Eq. (12) due to the electrostatic repulsion between BrO_3^- and TiO_2-P25 for pH values above 6.2, simultaneously with the absence, or occurrence in low extent, of BrO_3^- reduction by $O_2^{·-}$ and H_2O_2.

3.8. Influence of addition of HCOOH as OSA

HCOOH has been pointed out as a lead OSA for photocatalytic reductions of inorganic ions [31,32]. Marks et al. [33] reported an optimum initial [HCOOH]:[BrO_3^-] molar ratio close to 3:1 for photocatalytic trials with TiO_2-P90 in suspension. This initial [HCOOH]:[BrO_3^-] molar ratio was tested as well as molar ratios of 1:1 and 0.5:1.
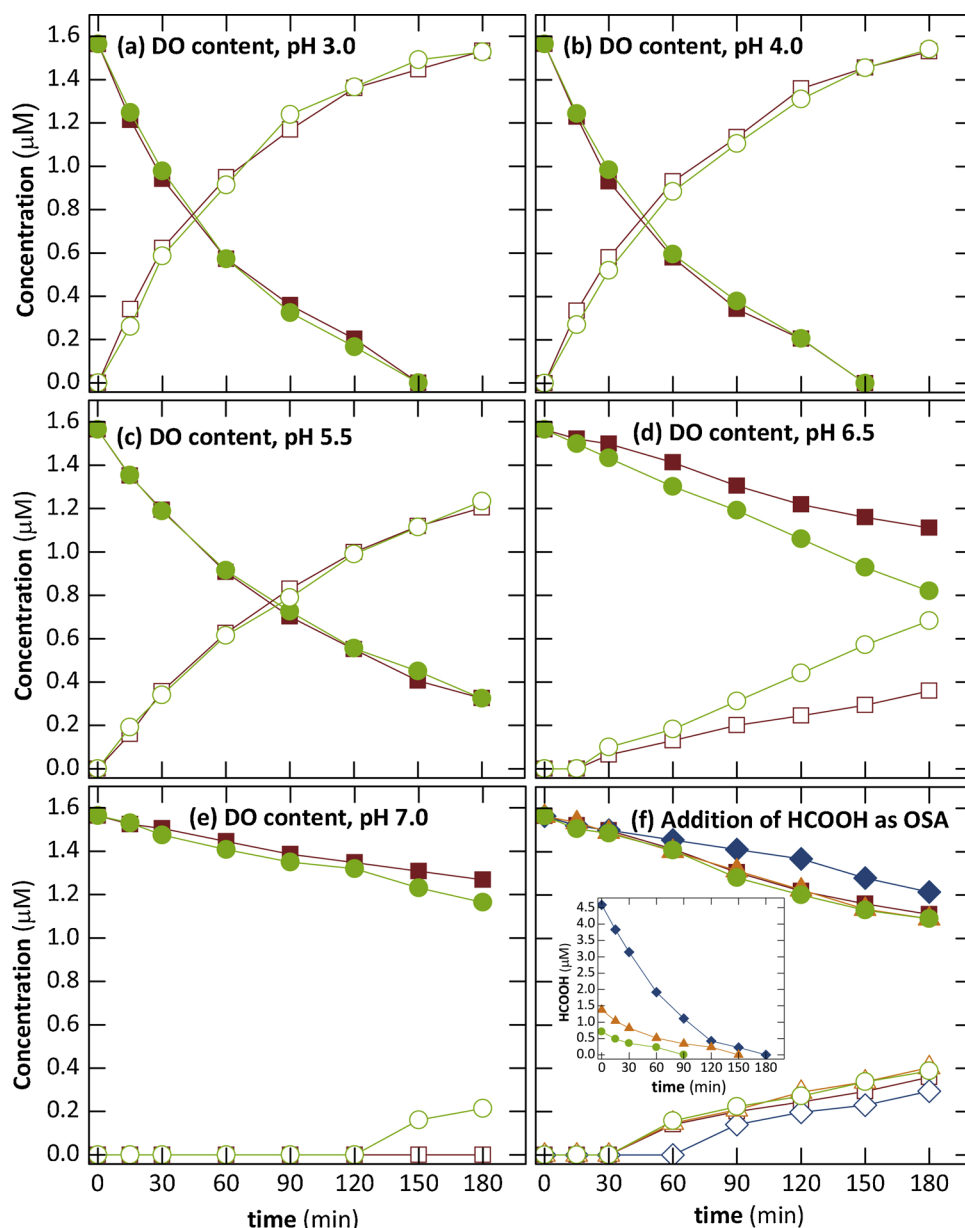
Fig. 5. Influence of DO content at pH 3.0 (a), 4.0 (b), 5.5 (c), 6.5 (d) and 7.0 (e) and addition of HCOOH as OSA (f) on BrO_3^- photocatalytic reduction. Solid symbols: BrO_3^-. Open symbols: Br^-. DO content: 212–239 μM (absence of N_2) (■,□), < 3.1 μM (presence of N_2) (●,○). [HCOOH]:[BrO_3^-] molar ratios: absence of HCOOH addition (■,□), 0.5:1 (●,○), 1:1 (▲,△), 3:1 (◆,◇) (conditions: Solution pH: 6.5; [DO]: 212–239 μM). General conditions: [BrO_3^-]$_0$: 1.56 μM; SM pre-treatment: SA[1] + IR[2] + TT[3]; SM position during dip coating: vertical; Number of photocatalyst layers: 6; Solution temperature: 25 °C. The inset panel of Fig. 5f exhibits the HCOOH concentration during reactions. [1]SA: Sandblast abrasion; [2]IR: Impurities removal; [3]TT: Thermal treatment.

Trials were carried out in the presence of DO contents of 212–239 μM and at pH 6.5 in an attempt to improve the BrO_3^- photocatalytic reduction at nearly neutral pH. Fig. 5f shows a lower BrO_3^- photocatalytic reduction rate using an initial [HCOOH]:[BrO_3^-] molar ratio of 3:1 when compared to the absence of HCOOH addition, along with a null process improvement for 1:1 and 0.5:1 [HCOOH]:[BrO_3^-] molar ratios. These results suggest the adsorption of high amounts of HCOOH onto the TiO_2-P25 surface for high HCOOH contents, thereby hindering a high fraction of UV photons to reach the photocatalyst surface and activate it, and impeding the most part of BrO_3^- to achieve the TiO_2-P25 surface and undergo photocatalytic reduction. For lower HCOOH concentrations, the blocking of the TiO_2-P25 surface by HCOOH may have occurred in lesser extent. This may have allowed a larger fraction of UV photons and BrO_3^- to reach the TiO_2-P25 surface, permitting the occurrence of some direct BrO_3^- photoreduction and/or to take advantage of the HCOOH presence benefits, such as BrO_3^- photoreduction by $CO_2^{\cdot-}$ and additional e_{CB}^-, and lower Br^- reoxidation to BrO_3^-. Dark experiments revealed the adsorption of 70–81% of the HCOOH onto system surfaces after 180 min of recirculation for the different initial [HCOOH]:[BrO_3^-] molar ratios at pH 6.5, confirming

the occurrence of HCOOH adsorption onto the TiO_2-P25 surface. HCOOH adsorption onto the TiO_2-P25 surface occurred despite the existence of some electrostatic repulsion between the negatively charged TiO_2-P25 and HCOOH (see Fig. SM-4) at pH 6.5.

Additional assays were carried out in the presence of DO contents < 3.1 μM and at pH 6.5 in the presence of DO contents of 212–239 μM (see Fig. SM-5). The HCOOH was unable to improve the BrO_3^- photocatalytic reduction regardless of the DO concentration and pH. Similar HCOOH dark adsorptions were achieved for both DO contents and a higher HCOOH adsorption of 100% after 150 min of recirculation was attained for pH 5.5. Since at pH 5.5 the TiO_2-P25 surface is positively charged and the HCOOH is negatively charged (Fig. SM-4), the higher HCOOH adsorption at pH 5.5 compared to pH 6.5 was expected.

3.9. Stability of the photocatalyst films

Consecutive trials in triplicate under distinct conditions achieved similar BrO_3^- reduction rates, indicating a constant activity of TiO_2-P25 thin films regardless of the SM pre-treatment, number of TiO_2-P25

layers, SM position during dip coating, solution pH, solution temperature, DO content and presence of HCOOH.

Moreover, Fig. SM-6 shows that a TiO_2-P25 film resulting from the deposition of 6 TiO_2-P25 layers on the vertically assembled and previously thermally treated SM was applied in twenty-five consecutive photocatalytic trials of 3 h without dropping its activity (75 h of operation). These results disclose the feasibility of applying non-uniform TiO_2-P25 thin films.

A $k_{bromate}$ decrease by 30% was achieved after subjecting the same TiO_2-P25 film to extreme mechanical stresses provided by 60 min of sonication at 37 kHz (Fig. SM-7 and Table 1). Taking into account that photocatalysis using the SM can be performed under laminar flow, a small friction between fluid and photocatalyst is expected, minimizing the detachment of the photocatalyst from the support.

4. Conclusions

BrO_3^- photocatalytic reduction to Br^- in pure aqueous solutions was successfully carried out by heterogeneous photocatalysis using TiO_2-P25 immobilized on a stainless steel Kenics® SM. The BrO_3^- photocatalytic reduction rate was mostly affected by the solution pH. The $k_{bromate}$ diminished by 93% when increasing pH from 4.0 to 7.0. TiO_2-P25 films characteristics also highly influenced the BrO_3^- photocatalytic reduction rate, with improved photocatalytic reductions being achieved for: (i) ticker TiO_2-P25 films up to the application of 6 TiO_2-P25 layers ($k_{bromate}$ differed by 43% from 1 to 6 layers), (ii) TiO_2-P25 films produced using the SM in the vertical position during the dip coating procedure instead of in the horizontal position ($k_{bromate}$ variation by 38%), and (iii) TiO_2-P25 films deposited on the thermally pretreated SM compared to the photocatalyst films deposited on the thermally/chemically pre-treated SM ($k_{bromate}$ variation by 33%). All the generated TiO_2-P25 films proved to be very stable, notwithstanding the non-uniformity of some of them. The DO had a negligible effect on the BrO_3^- photocatalytic reduction for solution pH values from 3.0 to 5.5 and a negative effect for higher pH values ($k_{bromate}$ variation by 42% and 24% at pH 6.5 and 7.0, respectively). Solution temperatures from 15 °C to 30 °C enhanced the BrO_3^- photocatalytic reduction rate ($k_{bromate}$ variation by 33%). Worse or similar BrO_3^- photocatalytic reduction rates were achieved in the presence of HCOOH addition at pH 5.5 and 6.5.

Acknowledgements

Appendix A. Supplementary data

Supplementary material related to this article can be found, in the online version, at doi:https://doi.org/10.1016/j.apcatb.2019.02.070.

References

[1] M. Flury, A. Papritz, Bromide in the natural environment: occurrence and toxicity, J. Environ. Qual. 22 (1993) 747–758, https://doi.org/10.2134/jeq1993. 00472425002200040017x.

[2] N.E. McTigue, D.A. Cornwell, K. Graf, R. Brown, Occurrence and consequences of increased bromide in drinking water sources, J. Am. Water Works Assoc. 106 (2014) E492–E508, https://doi.org/10.5942/jawwa.2014.106.0141.

[3] R. Butler, A. Godley, L. Lytton, E. Cartmell, Bromate environmental contamination: review of impact and possible treatment, Crit. Rev. Environ. Sci. Technol. 35 (2005) 193–217, https://doi.org/10.1080/10643380590917888.

[4] World Health Organization (WHO), Disinfectants and Disinfection By-Products, International Programme on Chemical Safety (IPCS), Environmental Health Criteria 216, Switzerland, 2000.

[5] International Agency for Research on Cancer (IARC), Some chemicals that cause tumours of the kidney or urinary bladder in rodents and some other substances, IARC Monogr. Eval. Carcinog. Risks Hum. 73 (1999) France.

[6] Portuguese Environment Council, Decree law 152/2017, Off. Gazette Portugal, Ser. I 235 (7) (2017) December 2017.

[7] The Council of the European Union (EU), Council Directive 98/83/EC of 3 November 1998 on the quality of water intended for human consumption, Off. J. Eur. Commun. (1998).

[8] United States Environmental Protection Agency (US EPA), National primary drinking water regulations: stage 2 Disinfectants and disinfection byproducts rule, Fed. Regist. 71 (2) (2006).

[9] World Health Organization (WHO), Guidelines for Drinking-water Quality, 4th edition, (2011) Switzerland.

[10] G.L. Amy, M.S. Siddiqui, Strategies to Control Bromate and Bromide, American Water Works Association (AWWA) and AWWA Research Foundation, United States of America, 1999.

[11] J. Coronado, F. Fresno, M.D. Hernández-Alonso, R. Portela, Design of advanced photocatalytic materials for energy and environmental applications, Green Energy Technol. (2013) Springer-Verlag London, United Kingdom.

[12] D.D. Dionysiou, G. Li Puma, J. Ye, J. Schneider, D. Bahnemann, Photocatalysis: Applications, The Royal Society of Chemistry, United Kingdom, 2016.

[13] D.R. Lide, Handbook of Chemistry and Physics, 84th edition, CRC Press, United States of America, 2004.

[14] A. Mills, A. Belghazi, D. Rodman, Bromate removal from drinking water by semiconductor photocatalysis, Water Res. 30 (1996) 1973–1978, https://doi.org/10. 1016/0043-1354(96)00012-7.

[15] F. Parrino, G. Camera-Roda, V. Loddo, V. Augugliaro, L. Palmisano, Photocatalytic ozonation: maximization of the reaction rate and control of undesired by-products, Appl. Catal. B: Environ. 178 (2015) 37–43, https://doi.org/10.1016/j.apcatb.2014. 10.081.

[16] X. Zhang, T. Zhang, J. Ng, J.H. Pan, D.D. Sun, Transformation of bromine species in TiO_2 photocatalytic system, Environ. Sci. Technol. 44 (2010) 439–444, https://doi. org/10.1021/es902592w.

[17] X. Huang, L. Wang, J. Zhou, N. Gao, Photocatalytic decomposition of bromate ion by the UV/P25-Graphene processes, Water Res. 57 (2014) 1–7, https://doi.org/10. 1016/j.watres.2014.02.042.

[18] H. Noguchi, A. Nakajima, T. Watanabe, K. Hashimoto, Removal of bromate ion from water using TiO_2 and alumina-loaded TiO_2 photocatalysts, Water Sci. Technol. 46 (2002) 27–31, https://doi.org/10.2166/wst.2002.0712.

[19] H. Noguchi, A. Nakajima, T. Watanabe, K. Hashimoto, Design of a photocatalyst for bromate decomposition: surface modification of TiO_2 by pseudo-boehmite, Environ. Sci. Technol. 37 (2003) 153–157, https://doi.org/10.1021/es0258733.

[20] J.C. Colmenares, Y.-J. Xu, Heterogeneous photocatalysis: from fundamentals to green applications, Green Chem. Sustain. Technol. (2016) Springer-Verlag Berlin Heidelberg, Germany.

[21] A.M. Díez, F.C. Moreira, B.A. Marinho, J.C.A. Espíndola, L.O. Paulista, M.A. Sanromán, M. Pazos, R.A.R. Boaventura, V.J.P. Vilar, A step forward in heterogeneous photocatalysis: process intensification by using a static mixer as catalyst support, Chem. Eng. J. 343 (2018) 597–606, https://doi.org/10.1016/j.cej.2018. 03.041.

[22] P. Rodriguez, V. Meille, S. Pallier, M. Ali Al Sawah, Deposition and characterisation of TiO_2 coatings on various supports for structured (photo)catalytic reactors, Appl. Catal. A Gen. 360 (2009) 154–162, https://doi.org/10.1016/j.apcata.2009.03.013.

[23] A.J. Nozik, Photoelectrochemistry: applications to solar energy conversion, Annu. Rev. Phys. Chem. 29 (1978) 189–222, https://doi.org/10.1146/annurev.pc.29. 100178.001201.

[24] S.T. Martin, H. Herrmann, M.R. Hoffmann, Time-resolved microwave conductivity. Part 2. Quantum-sized TiO_2 and the effect of adsorbates and light intensity on charge-carrier dynamics, J. Chem. Soc. Faraday Trans. 90 (1994) 3323–3330, https://doi.org/10.1039/FT9949003323.

[25] D.A. Armstrong, R.E. Huie, W.H. Koppenol, S.V. Lymar, G. Merényi, P. Neta, B. Ruscic, D.M. Stanbury, S. Steenken, P. Wardman, Standard electrode potentials involving radicals in aqueous solution: inorganic radicals (IUPAC Technical Report), Pure Appl. Chem. 87 (2015) 1139–1150, https://doi.org/10.1515/pac-2014-0502.

[26] A. Pardo, M.C. Merino, A.E. Coy, F. Viejo, R. Arrabal, E. Matykina, Effect of Mo and Mn additions on the corrosion behaviour of AISI 304 and 316 stainless steels in H_2SO_4, Corros. Sci. 50 (2008) 780–794, https://doi.org/10.1016/j.corsci.2007.11. 004.

[27] K. Suttiponparnit, J. Jiang, M. Sahu, S. Suvachittanont, T. Charinpanitkul, P. Biswas, Role of surface area, primary particle size, and crystal phase on titanium dioxide nanoparticle dispersion properties, Nanoscale Res. Lett. 6 (2010) 27, https://doi.org/10.1007/s11671-010-9772-1.

[28] K.-Y.A. Lin, C.-H. Lin, S.-Y. Chen, H. Yang, Enhanced photocatalytic reduction of concentrated bromate in the presence of alcohols, Chem. Eng. J. 303 (2016)

596–603, https://doi.org/10.1016/j.cej.2016.06.056.

[29] Y. Zhang, L. Li, H. Liu, T. Lu, Graphene oxide and F co-doped TiO_2 with (001) facets for the photocatalytic reduction of bromate: synthesis, characterization and reactivity, Chem. Eng. J. 307 (2017) 860–867, https://doi.org/10.1016/j.cej.2016.08.139.

[30] S. Arrhenius, Über die Dissociationswärme und den Einfluss der Temperatur auf den Dissociationsgrad der Elektrolyte, Z. Phys. Chem. 4U (1889) 96, https://doi.org/10.1515/zpch-1889-0408.

[31] V.N.H. Nguyen, R. Amal, D. Beydoun, Effect of formate and methanol on photoreduction/removal of toxic cadmium ions using TiO_2 semiconductor as photocatalyst, Chem. Eng. Sci. 58 (2003) 4429–4439, https://doi.org/10.1016/S0009-2509(03)00336-1.

[32] T. Tan, D. Beydoun, R. Amal, Effects of organic hole scavengers on the photocatalytic reduction of selenium anions, J. Photochem. Photobiol. A Chem. 159 (2003) 273–280, https://doi.org/10.1016/S1010-6030(03)00171-0.

[33] R. Marks, T. Yang, P. Westerhoff, K. Doudrick, Comparative analysis of the photocatalytic reduction of drinking water oxoanions using titanium dioxide, Water Res. 104 (2016) 11–19, https://doi.org/10.1016/j.watres.2016.07.052.